Supporting Information

Compressive-strain-facilitated fast oxygen migration with reversible topotactic transformation in $La_{0.5}Sr_{0.5}CoO_x$ via all-solid-state electrolyte gating

Zhuo Yin[†,‡], Jianlin Wang[†,‡], Jing Wang*[,†,‡,▽], Jia Li[†,‡], Houbo Zhou[†,‡], Cheng Zhang[†,‡], Hui Zhang[⊥], Jine Zhang[⊥], Feiran Shen[&,‖], Jiazheng Hao[&,‖], Zibing Yu[†,‡], Yihong Gao[†,‡], Yangxin Wang[†,‖], Yunzhong Chen[†], Ji-Rong Sun[†,‡,§], Xuedong Bai*[,†,‡,§], Jian-Tao Wang*[,†,‡,§], Fengxia Hu*[,†,‡,§], Tong-Yun Zhao[†,o], Baogen Shen*[,†,‡,◊,o]

[†]Beijing National Laboratory for Condensed Matter physics, Institute of Physics, Chinese Academy of Sciences, Beijing 100190, China

[‡]School of Physical Sciences, University of Chinese Academy of Sciences, Beijing 101408, China

[▽]Fujian Innovation Academy, Chinese Academy of Sciences, Fuzhou, Fujian 350108, China

[⊥]School of Integrated Circuit Science and Engineering, Beihang University, Beijing 100191, China

[&]Institute of High Energy Physics, Chinese Academy of Sciences, Beijing 100049, China

[‖]Spallation Neutron Source Science Center, Dongguan 523803, China

[§]Songshan Lake Materials Laboratory, Dongguan, Guangdong 523808, China

[◊]Ningbo Institute of Materials Technology & Engineering, Chinese Academy of Sciences, Ningbo, Zhejiang, 315201, China

[o]Ganjiang Innovation Academy, Chinese Academy of Sciences, Ganzhou, Jiangxi, 341000, China

Series title:

SI-1. Stability of perovskite and brownmillerite phases in $La_{0.5}Sr_{0.5}CoO_x$

It has been reported that the perovskite $SrCoO_3$ and brownmillerite $LaCoO_{2.5}$ are not structurally stable when exposed to the air in previous study[S1,S2]. However, after 60 days of exposure to the air, the diffraction peak of presented $La_{0.5}Sr_{0.5}Co_3$ (red dashed line in Fig.S1a) and $La_{0.5}Sr_{0.5}Co_{2.5}$ (blue dashed line in Fig.S1b) still remain unchanged. This suggests that the perovskite and brownmillerite phases are stable in $La_{0.5}Sr_{0.5}CoO_x$ system, which provides a stable platform for the study of two-state switching and memory devices.

In order to understand the stability of the brownmillerite and perovskite phase of $La_{0.5}Sr_{0.5}CoO_x$, we have calculated the energy difference ($\Delta E = E(\mathrm{ABO_3}) - [E(\mathrm{ABO_{2.5}}) + \frac{1}{4}E(\mathrm{O_2})]$) of cubic $SrCoO_3$, $LaCoO_3$, and $La_{0.5}Sr_{0.5}CoO_3$ phase by using DFT, compared to the orthorhombic $SrCoO_{2.5}$, $LaCoO_{2.5}$, and $La_{0.5}Sr_{0.5}CoO_{2.5}$ phase, respectively, with an equation of $E(\mathrm{ABO_{2.5}}) + \frac{1}{4}E(\mathrm{O_2}) \rightarrow E(\mathrm{ABO_3})$, where $E(\mathrm{O_2})/4$ is calculated to be -2.417 eV. The calculated total energy are listed in Table S1. The energy difference ($\triangle E$) is calculated to be 0.235 eV for $SrCoO_3$, -0.549 eV for $LaCoO_3$, and -0.055 eV for $La_{0.5}Sr_{0.5}CoO_3$, respectively. We can see that the cubic perovskite $SrCoO_3$ phase is unstable and more like to form brownmillerite $SrCoO_{2.5}$ phase, while cubic perovskite $LaCoO_3$ phase is stable than the brownmillerite phase with a large energy gain of -0.549 eV. Meanwhile, cubic perovskite $La_{0.5}Sr_{0.5}CoO_3$ is also more stable than the brownmillerite phase $La_{0.5}Sr_{0.5}CoO_{2.5}$, which leads to a higher reaction barrier from cubic to orthorhombic phase than the reverse reaction with a barrier difference of 0.055 eV. However, the formation energy (-0.055 eV) is one order of magnitude smaller than those of $SrCoO_3$, and $LaCoO_3$, suggesting that the transition between brownmillerite $La_{0.5}Sr_{0.5}CoO_{2.5}$ and perovskite phases $La_{0.5}Sr_{0.5}CoO_3$ can be easily reversible under external stimulations (such as external electric field in this work).

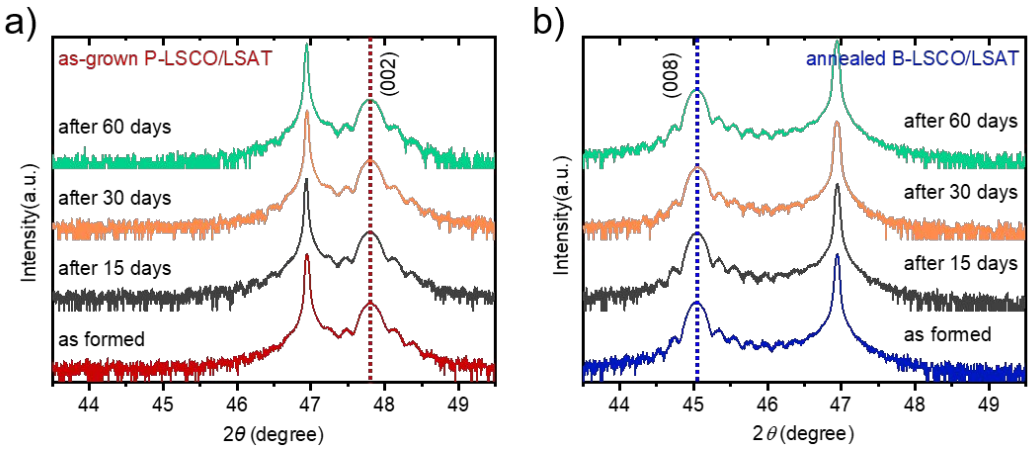

Fig. S1. Structural stability for a) as-grown P-LSCO and b) vacuum-annealed B-LSCO exposed to the air.

Table S1 The calculated total energy (E) and energy difference (ΔE) for $LaCoO_x$, $SrCoO_x$ and $La_{0.5}Sr_{0.5}CoO_x$.

E ($SrCoO_{2.5}$)	E ($SrCoO_{2.5}$)+$\frac{1}{4}E(O_2)$	E ($SrCoO_3$)	$\Delta E = E(SrCoO_3) - [E(SrCoO_{2.5}) + \frac{1}{4}E(O_2)]$	
-27.7813 eV	-30.1983 eV	-29.9638 eV	0.235 eV > 0	$SrCoO_{2.5}$ is more stable.
E ($LaCoO_{2.5}$)	E ($LaCoO_{2.5}$)+$\frac{1}{4}E(O_2)$	E ($LaCoO_3$)	$\Delta E = E(LaCoO_3) - [E(LaCoO_{2.5}) + \frac{1}{4}E(O_2)]$	
-32.9984 eV	-35.4153 eV	-35.9638 eV	-0.549 eV < 0	$LaCoO_3$ is more stable.
E ($La_{0.5}Sr_{0.5}CoO_{2.5}$)	E ($La_{0.5}Sr_{0.5}CoO_{2.5}$)+$\frac{1}{4}E(O_2)$	E ($La_{0.5}Sr_{0.5}CoO_3$)	$\Delta E = E(La_{0.5}Sr_{0.5}CoO_3) - [E(La_{0.5}Sr_{0.5}CoO_{2.5}) + \frac{1}{4}E(O_2)]$	
-30.4604 eV	-32.8774 eV	-32.9329 eV	-0.055 eV < 0	$La_{0.5}Sr_{0.5}CoO_3$ is more stable

SI-2. Surface topography and epitaxial quality of as-grown P-LSCO films

The quality and morphology of the film could largely affect the gating-modulation progress. To evaluate the possible influence of surface morphology, we performed the atomic force microscopy (AFM) measurements for all the as-grown P-LSCO films on various substrates. All results are shown in Fig.S2. Firstly, all films exhibit similar surface morphology, no special feature such as obvious nanoparticles are observed on the surface. Meanwhile, the calculated root mean square (RMS) surface roughness of films on different substrates are all below 7.0 Å and within a small range of from 2.7 Å to 6.5 Å (Fig.S2). These results demonstrate that these films on different substrates have alike and good surface morphology.

Moreover, the small angle X-ray reflection (XRR) measurements were also carried out to check the quality of films on five substrates. The collected results and fitting data are plotted in Fig.S3. Firstly, almost same thicknesses (~40 nm) are determined for all films (Fig.S3f). The clear periodic oscillation in the reflection curve evidences the smooth interface/surface of films (Note that the inconspicuous oscillation for P-LSCO/LAO is caused by the similar mass densities between $La_{0.5}Sr_{0.5}CoO_3$ (6.54 g/cm3) and LAO (6.52 g/cm3)). Furthermore, the almost same depth profile of X-ray scattering length density (SLD) for all films (see inset of Fig.S3), obtained by fitting the reflection curves, indicates that our films on different substrates have uniform chemical composition.[S3] In addition, the measurements of X-ray diffraction rocking curve for films on different substrates were performed to further compare the film quality. Results of P-LSCO on various substrates of LAO, NGO, LSAT and STO are plotted in Fig.S4, respectively. It was found that the full width at half maximum (FWHM) of all curves are very small, ranging from 0.04° to 0.08°, evidencing that all films have the same and good epitaxial quality.

All these results demonstrate that the presented films on different substrates have good epitaxial quality and similar surface topography. Thus the influence of the surface morphology and film quality on the observed strain-dependent gating-modulation may be trivial.

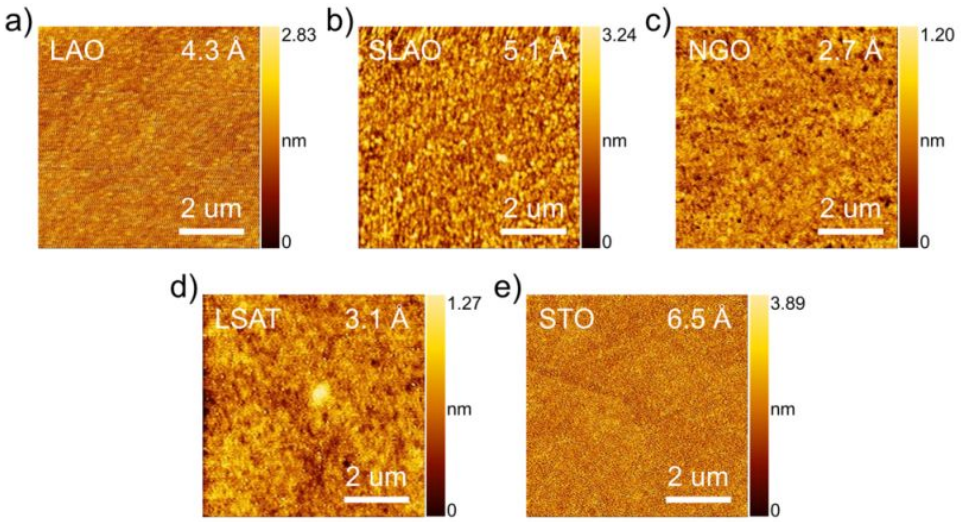

Fig. S2. AFM measurements of as-grown P-LSCO on five substrates of a) LAO, b) SLAO, c) NGO, d) LSAT and f) STO. The specific RMS surface roughness is written on the image of each film.

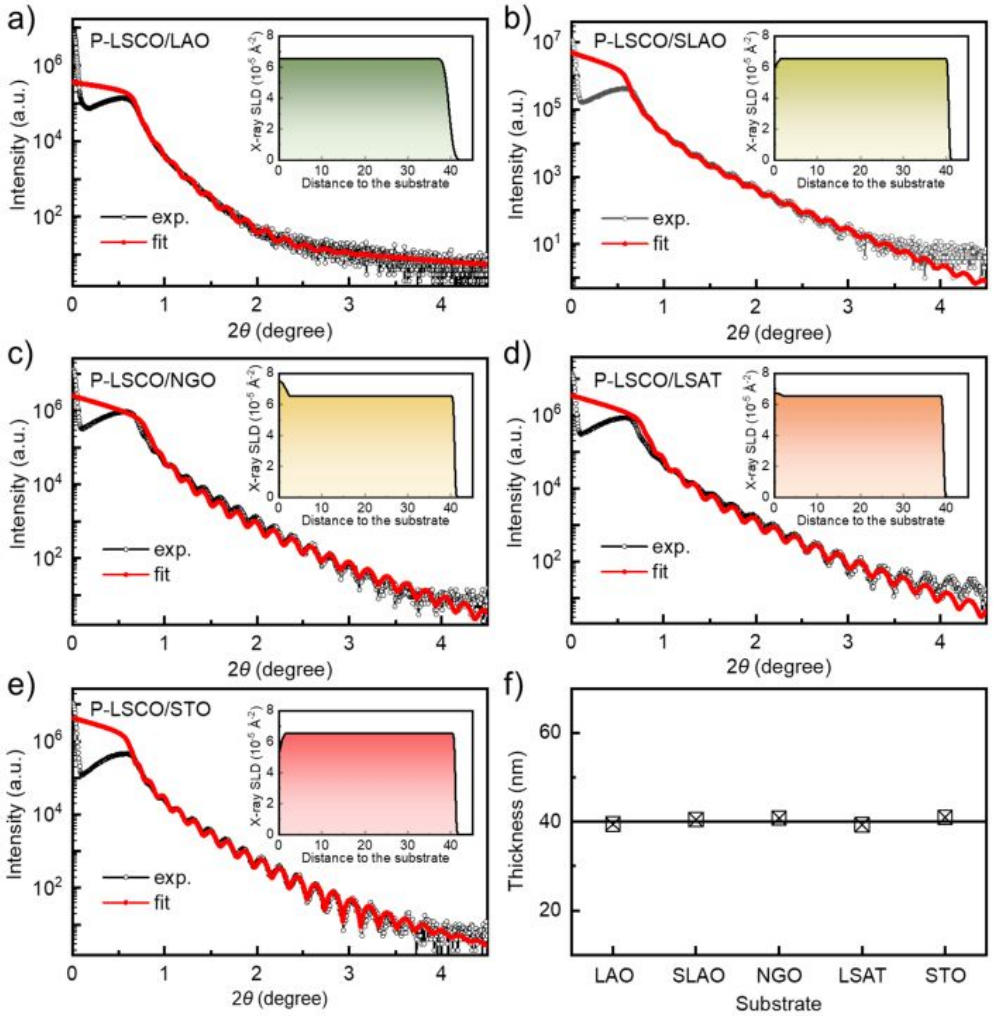

Fig. S3. Small angle XRR and corresponding data fit for as-grown P-LSCO/STO films on substrates of a) LAO, b) SLAO, c) NGO, d) LSAT and e) STO, respectively. The insets are X-ray SLD depth profile as a function of the distance obtained by fitting the reflection curves. f) The obtained film thicknesses for five films.

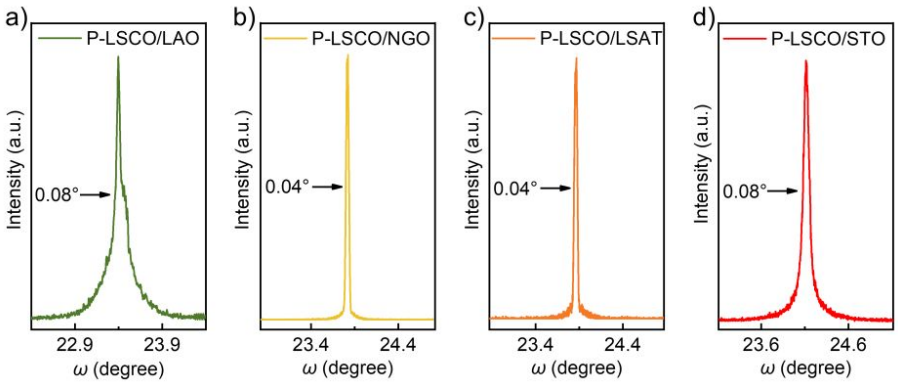

Fig. S4. X-ray diffraction rocking curves of P-LSCO films on substrates of a) LAO, b) NGO, c) LSAT and d) STO, respectively. All curves show a very small FWHM with the rang from 0.04° to 0.08°, indicating the same and good quality for films on different substrates.

SI-3. Crystal structural characterization and acquisition of in-plane lattice strain of films

The $La_{0.5}Sr_{0.5}CoO_3$ films about 40 nm thickness on five substrates were deposited and the thickness was accurately measured by small angle XRR (Fig.S3f). We use XRD θ-2θ scans to identify the crystal structures of as-grown and vacuum-annealed films (perovskite and brownmillerite phases). For the as-grown P-LSCO films on five substrates, characteristic diffraction peaks of typical perovskite structure ((001), (002), (003)) are observed (Fig.S5a). While for the annealed B-LSCO films, the (002), (004), (006), (008), (00$\underline{1}$0) diffraction peaks emerge (Fig.S5b), indicating a brownmillerite phase. All the films are single phases. In addition, the positions of diffraction peak of P- and B-LSCO gradually shift to high angle from LSCO/LAO to LSCO/STO (enlarged pattern (42-50°) in Fig.S5a, b), which corresponds to a gradual decrease in out-of-plane lattice parameter of film (c_{film}) due to lattice mismatch between LSCO film and substrates.

The IP lattice strain of films (ε) are calculated by the equation $\varepsilon = (a_{film}-a_{bulk})/a_{bulk}$, where a_{bulk} is the lattice parameter of bulk $La_{0.5}Sr_{0.5}CoO_3$ (3.842 Å). The lattice parameter of the film a_{film} is obtained from X-ray RSM ($a_{film} = 1/q_x$, q_x is reciprocal space vector). The miller indexes are set as ($\underline{-}$103) for LAO, NGO, LSAT, STO but ($\underline{-}$10$\underline{1}$1) for SLAO in RSM measurement. All calculated values of ε are given in Table 1.

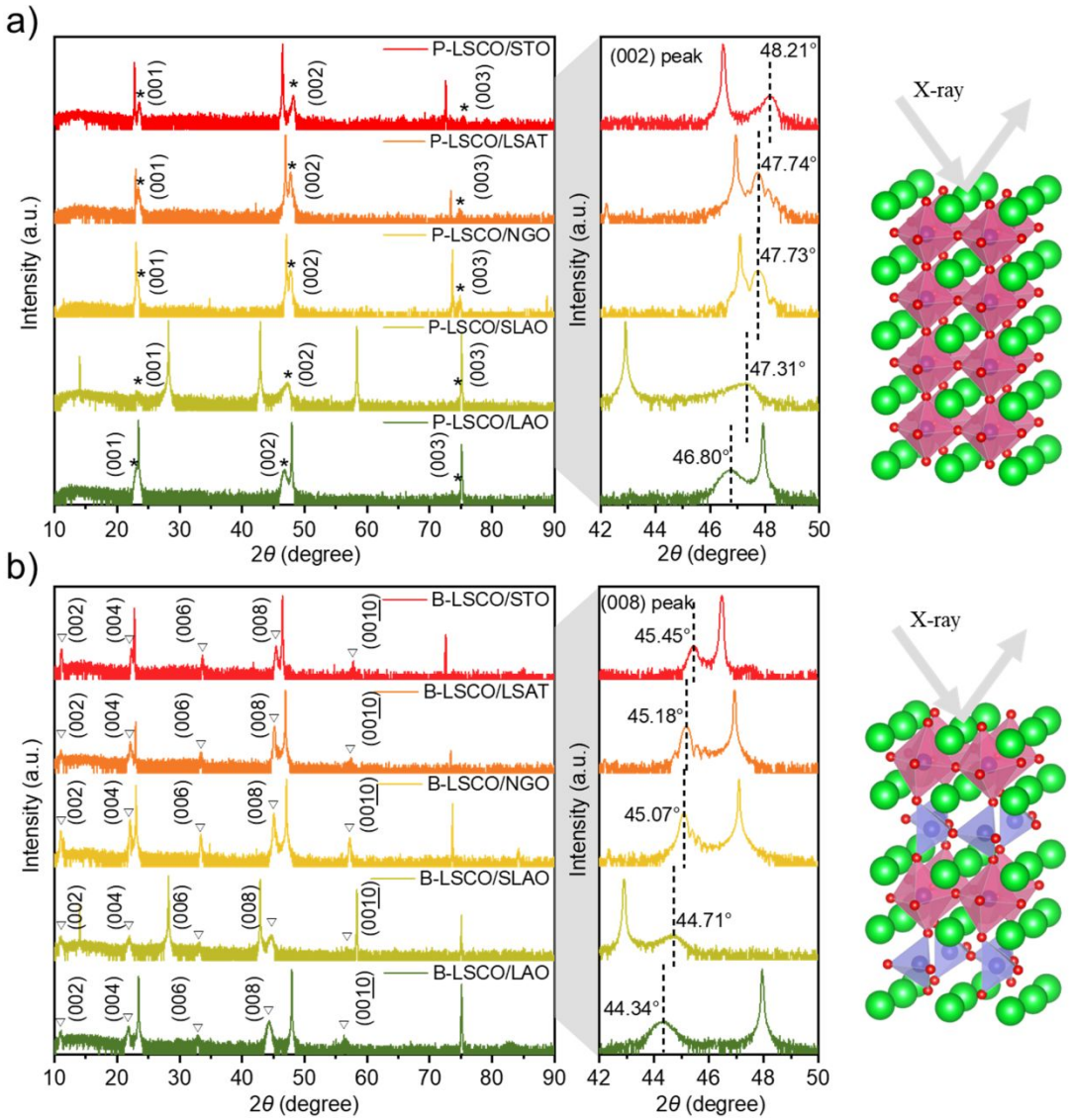

Fig. S5 a) XRD θ-2θ scans pattern (10-90°) and enlarged pattern (42-50°) of as-grown P-LSCO films on five substrates. b) XRD θ-2θ scans (10-90°) pattern and enlarged pattern (42-50°) of vacuum-annealed B-LSCO films on five substrates.

SI-4. Reversible topological phase transformation for LSCO/SLAO, LSCO/NGO and LSCO/LSAT

The reversible topological phase transformation (RTPT) for LSCO/SLAO (ε = -0.42 %), LSCO/NGO (ε = +0.57 %), and LSCO/LSAT (ε = +0.68 %) by IG gating-modulation are achieved commendably. When +2V gate-voltage is applied to P-LSCO films (Fig.S6a, b, c, blue line), O^{2-}-ions migrate out of the film, leading to formation of ordered superstructure in the film. Finally, the film transforms to B-LSCO, showing characteristic XRD peaks of browmillertie phase as same as the vacuum-annealed B-LSCO (11.0°-(002), 22.0°-(004), 33.1°-(006), 44.7°-(008) and 56.8°-(00$\underline{1}$0) for +2V-gating modulated B-LSCO/SLAO, 11.0°, 22.1°, 33.4°, 45.1° and 57.2° for +2V-gating modulated B-LSCO/NGO, 11.1°, 22.1°, 33.4°, 45.2° and 57.4° for +2V-gating modulated B-LSCO/LSAT).

When reversed -3V gate-voltage is applied (Fig.S6a, b, c, red line), O^{2-}-ions migrate into film orderly, the film reverts back into P-LSCO phase, with XRD characteristic peaks at 23.1°-(001) and 47.3°-(002) for -3V-gating modulated P-LSCO/SLAO (23.2° and 47.7° for -3V-gating modulated P-LSCO/NGO, 23.5° and 47.8° for -3V-gating modulated P-LSCO/LSAT), same as as-grown P-LSCO. These results demonstrate completed RTPTs based on all-solid-state IG gating-modulation.

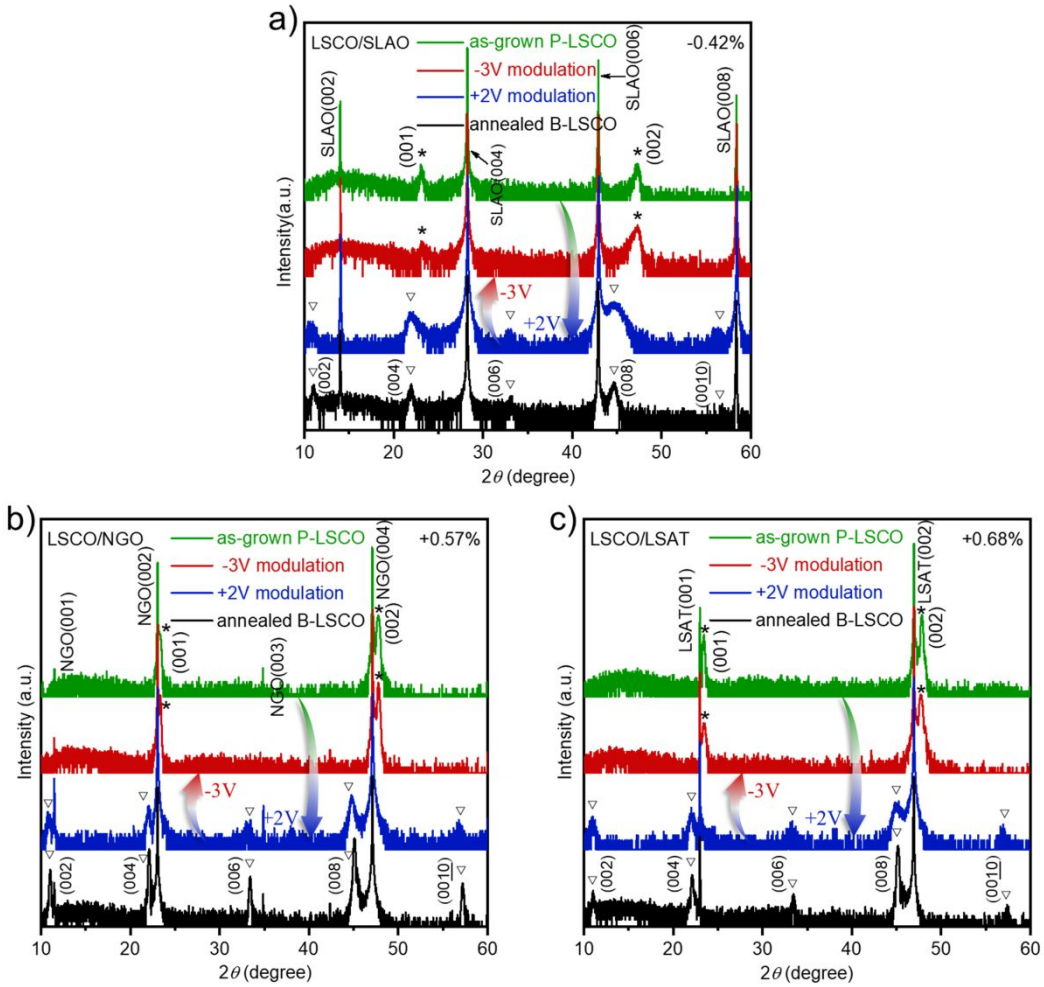

Fig. S6 RTPTs for a) LSCO/SLAO. b) LSCO/NGO. c) LSCO/LSAT. The green trace is as-grown P-LSCO, the black trace is annealed B-LSCO, the blue trace is for the film after +2V gating-modulation from as-grown P-LSCO, and the red trace is after -3V gating-modulation from +2V gating modulated B-LSCO.

SI-5. Stability of reversible topological phase transitions via gating-modulation

Serial modulation experiments were performed to evaluate the reversible stability of topotactic transformation by ionic gel (IG) gating-modulation. The XRD results after four cycles of oxygen insertion and extraction for the LSCO/LAO film are illustrate in Fig.S7. One can find that the topological phase transformation between brownmillerite and perovskite phase were achieved in all cycles, indicating that the transformation by gating-modulation is completely reversible. In each cycle, after applying +2V gating-voltage on P-LSCO/LAO film, the characteristic (008) superstructure diffraction peak of brownmillerite phase (B-phase) appears at 44.3° accompanied with the disappearance of the (002) diffraction peak of perovskite phase (P-phase), demonstrating the transformation from P- to B-phase due to the oxygen extraction. Reversely, after subsequently applying -3V gating-voltage on B-LSCO/LAO film, the (002) diffraction peak of P-phase re-appears at 46.8° with the disappearance of (008) characteristic diffraction peak of B-phase due to the oxygen insertion. Moreover, the intensity and position of characteristic peak of both P-phase and B-phase remain almost unchanged in each cycle (see Fig.S7). These results evidence that the gating-modulated topotactic transformation in present LSCO films has a good reversible stability.

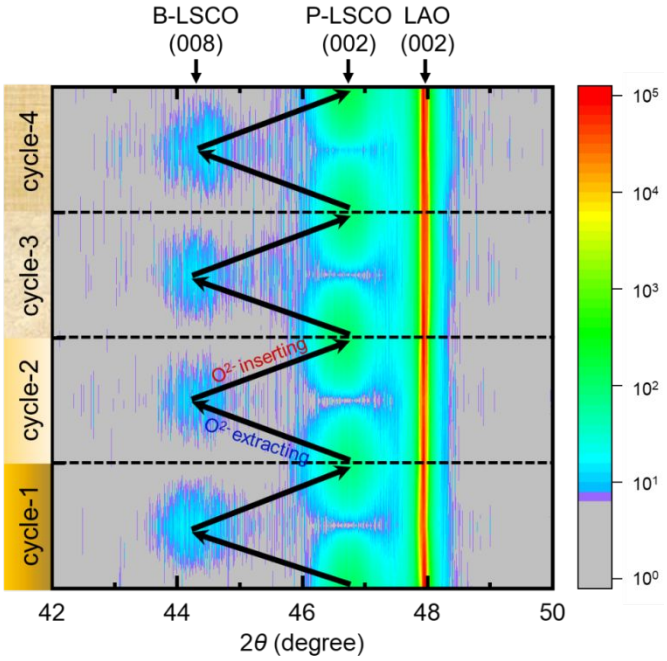

Fig. S7. XRD patterns of the LSCO/LAO film upon successively applying +2V (oxygen extraction) and -3V (oxygen insertion) gating-voltage in 4 cycles.

SI-6. Transition energy between P and B phases with strains based on thin films

To understand the relative stability of the perovskite (P) and brownmillerite (B) phase in strained films, we have calculated the transition energy between P and B phases ($\Delta E = E(La_{0.5}Sr_{0.5}CoO_3) - [E(La_{0.5}Sr_{0.5}CoO_{2.5}) + \frac{1}{4}E(O_2)]$) with varying strains of thin films by using DFT calculation. The lattice parameters *b* and *c* for both P and B phases are set to be 5.442, 5.470, 5.522, 5.57, 5.62, 5.68, and 5.75 Å, while the lattice parameter *a* and atomic positions are full relaxed. The transition energy ΔE is calculated to be -0.138, -0.130, -0.114, -0.097, -0.077, -0.049, -0.010 eV for the system with strain ε varying from to -3.3 % to 2.2 %, respectively. The result is plotted in Fig.S8. We can see that the transition energy remains below zero within the whole strain range, which means that the P-phase is more favorable and stable than B-phase even under tensile or compressive strains. This result further verifies that the transition from B- to P-LSCO in strained-films is more efficient and well consistent with the smaller t_{du} in the process of B- to P-LSCO. Moreover, one can find that tensile strain induces an increasing of the transition energy from -0.077 to -0.010 eV, while the compressive strain results in a decreasing of the transition energy from -0.077 to -0.138 eV. This means that the stability difference between P-phase and B-phase decreases with the strain changing from compressive -3.3 % to tensile +2.2 %, which is consistent with the gradual reduction in the directional discrepancy of t_{du} (see Fig.2d).

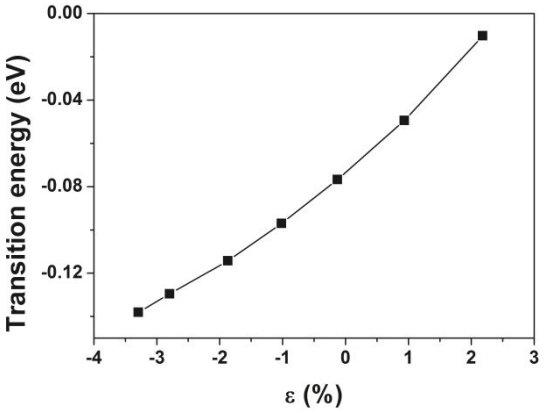

Fig. S8. The transition energy between P- and B-LSCO as a function of strain ε.

SI-7. Magnetic and electrical transport measurements for as-grown P-LSCO/STO

We have performed measurements on the as-grown P-LSCO/STO film and the obtained magnetic and electrical transport data was illustrated in Fig.S9. It can be seen that the as-grown film exhibits a distinct ferromagnetic insulating behavior with a Curie temperature T_c of 203 K and saturated magnetization M_s of 1.31 μ_B/Co (at $\mu_0 H$ = 5 T), which is consistent with the gating-modulated P-LSCO/STO (T_c ~ 206 K, M_s ~ 1.35 μ_B/Co) (see Fig.S9 and Fig.3). These results indicate that observed unusual ferromagnetic insulator (FMI) is an intrinsic characteristic for presented P-LSCO/STO film. Previously, D. Meng et al.[S4] has reported a perovskite ferromagnetic insulator in tensile-strained $LaCoO_3$ single crystalline thin films, which was ascribed to the tensile strain induced FM coupling between nearest high-spin and low-spin Co ions.[S5, S6] Considering the same crystalline structure and similar ferromagnetism origin in present LSCO films, it is reasonable to attribute the observed similar ferromagnetic insulator to the large tensile strain in LSCO/STO film (+1.64 %).

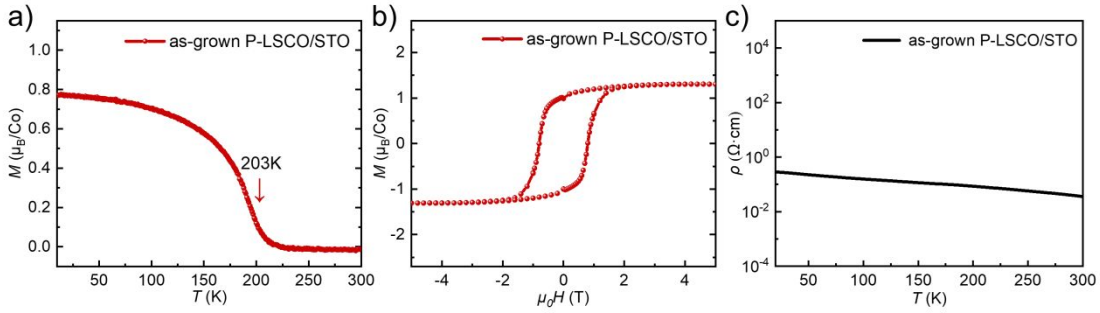

Fig. S9. Magnetic and electrical transport measurements for as-grown P-LSCO/STO. a) Temperature dependence of magnetization M (T) curves under field cooling with applying an in-plane magnetic field $\mu_0 H$ = 0.05 T, where the arrow marks the Curie temperature (T_c). b) Magnetic hysteresis loops M (H) measured at 10 K. c) Resistivity (ρ) as a function of temperature.

SI-8. Diffusion of single oxygen atom in brownmillerite $La_{0.5}Sr_{0.5}CoO_{2.5}$

To understand the insertion and extraction process of O^{2-}-ions, we have calculated the energy profiles of single O-atom diffusion in the vacancy line of orthorhombic $La_{0.5}Sr_{0.5}CoO_{2.5}$ phase using the CI-NEB method.[S7] The diffusion pathways along the z-direction [from site (0.5, *y*, 0) to site (0.5, *y*, 1)] and corresponding energy profiles are presented in Fig.S10. The lattice parameters *b* and *c* for brownmillerite $La_{0.5}Sr_{0.5}CoO_{2.5}$ phase used in the calculation are set to be 5.442, 5.470, 5.522, 5.57, 5.62, 5.68, and 5.75 Å from line-1 to line-7, respectively, while the lattice parameter *a* = 15.7724 Å is fixed. The calculated diffusion barrier is 0.647, 0.629, 0.614, 0.646, 0.694, 0.782, and 0.915 eV from line-1 to line-7, respectively. We can see that tensile strain induces an increasing of the diffusion barrier from 0.614 to 0.915 eV. This means that a longer time and higher energy are needed for the insertion or extraction process of O^-atom under tensile-strain.

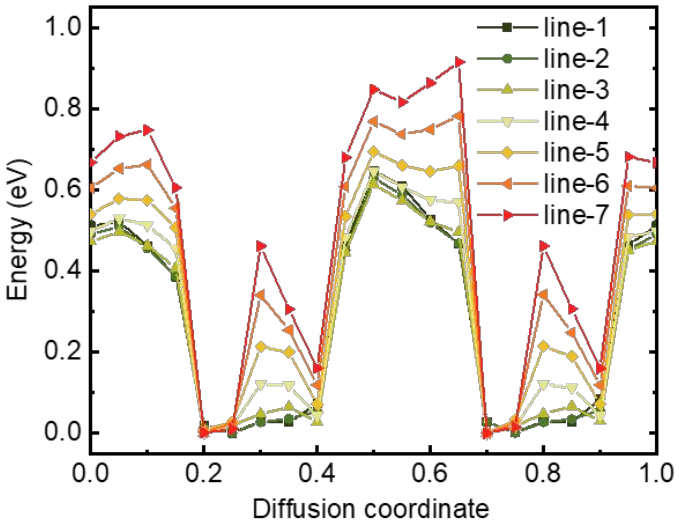

Fig. S10 Diffusion of single O-atom in brownmillerite $La_{0.5}Sr_{0.5}CoO_{2.5}$. The diffusion coordinate (z) is changed from 0 to 1.

SI-9. Calculation for sXAS Co L_3/L_2 ratio

To evaluate the variation of Co-ions valence state in modulated B-LSCO films with lattice strain, the L_3/L_2 ratio is calculated by area ratio of L_3 and L_2 peaks (shadow area-A and -B in Fig.S11). The integral range of the peak is set as 10 eV. A background intensity is deducted prior to the integration, which is modeled by step functions in the threshold regions roughly (pink line in Fig.S11). The ratio of the step heights is chosen to be 2 : 1 (2/3*h* and 1/3*h*) in accordance with the multiplicity of the initial states (four 2*p*3/2 electrons and two 2*p*1/2 electrons).[S8-S11] This background subtraction procedure is followed consistently for all of the acquired spectra.

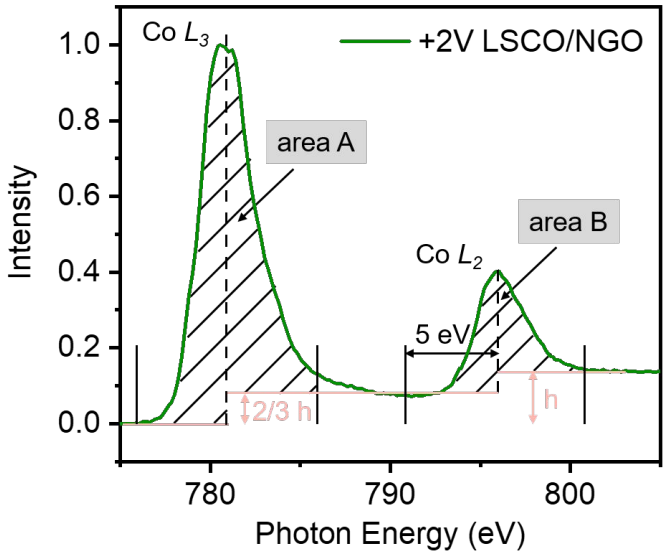

Fig. S11 Calculation sXAS for Co L_3/L_2 ratio.

REFERENCES:

S1. Huang, H.; Zhang, J.; Zhang, H.; Han, F.; Chen, X.; Song, J.; Zhang, J.; Qi, S.; Chen, Y.; Cai, J.; Hu, F.; Shen, B.; Sun, J. Topotactic Transition between Perovskite and Brownmillerite Phases for Epitaxial $LaCoO_{3-\delta}$ Films and Effects thus Resulted. *J. Phys. D: Appl. Phys.* **2020**, *53*, 155003.

S2. Lu, N.; Zhang, P.; Zhang, Q.; Qiao, R.; He, Q.; Li, H. B.; Wang, Y.; Guo, J.; Zhang, D.; Duan, Z.; Li, Z.; Wang, M.; Yang, S.; Yan, M.; Arenholz, E.; Zhou, S.; Yang, W.; Gu, L.; Nan, C. W.; Yu, P.; et al. Electric-Field Control of Tri-State Phase Transformation with a Selective Dual-Ion Switch. *Nature* **2017**, *546*, 124-128.

S3. Li H.; Yang Y.; Deng S.; Zhang L.; Cheng S.; Guo E.-J.; Zhu T.; Wang H.; Wang J.; Wu M.; Gao P.; Xiang H.; Xing X.; Chen J. Role of Oxygen Vacancies in Colossal Polarization in $SmFeO_{3-\delta}$ Thin Films. *Sci. Adv.* **2022**, *8*, 8550.

S4. Meng D.; Guo H.; Cui Z.; Ma C.; Zhao J.; Lu J.; Xu H.; Wang Z.; Hu X.; Fu Z.; Peng R.; Guo J.; Zhai X. F.; Brown G. J.; Knize R.; Lu Y. Strain-Induced High-Temperature Perovskite Ferromagnetic Insulator. *Proc. Natl. Acad. Sci. U. S. A.* **2018**, *115*, 2873-2877.

S5. Hsu, H.; Blaha, P.; Wentzcovitch, R. M. Ferromagnetic Insulating State in Tensile-Strained $LaCoO_3$ Thin Films from LDA+*U* Calculations. *Phys. Rev. B* **2012**, *85*, 140404.

S6. Seo, H.; Posadas, A.; Demkov, A. A. Strain-Driven Spin-State Transition and Superexchange Interaction in $LaCoO_3$: *Ab Initio* Study. *Phys. Rev. B* **2012**, *86*, 014430.

S7. Henkelman, G.; Jonsson, H. Improved Tangent Estimate in the Nudged Elastic Band Method for Finding Minimum Energy Paths and Saddle Points. *J. Chem. Phys.* **2000**, *113*, 9978-9985.

S8. Pearson, D. H.; Ahn, C. C.; Fultz, B. White Lines and D-Electron Occupancies for the 3*d* and 4*d* Transition-Metals. *Phys. Rev. B* **1993**, *47*, 8471-8478.

S9. Kurata, H.; Colliex, C. Electron-Energy-Loss Core-Edge Structures in Manganese Oxides. *Phys. Rev. B* **1993**, *48*, 2102-2108.

S10. Botton, G. A.; Appel, C. C.; Horsewell, A.; Stobbs, W. M. Quantification of the EELS Near-Edge Structures to Study Mn Doping in Oxides. *J. Microscopy-Oxford* **1995**, *180*, 211-216.

S11. Lloyd, S. J.; Botton, G. A.; Stobbs, W. M. Changes in the Iron White-Line Ratio in the Electron Energy-Loss Spectrum of Iron-Copper Multilayers. *J. Micro.* **1995**, *180*, 288-293.